



**HAL**  
open science

## Signatures of projectile nucleus scattering in three-dimensional (e,2e) cross sections for argon

Xueguang Ren, Arne Senftleben, Thomas Pflüger, Alexander Dorn, Klaus  
Bartschat, Joachim Ullrich

► **To cite this version:**

Xueguang Ren, Arne Senftleben, Thomas Pflüger, Alexander Dorn, Klaus Bartschat, et al.. Signatures of projectile nucleus scattering in three-dimensional (e,2e) cross sections for argon. *Journal of Physics B: Atomic, Molecular and Optical Physics*, 2010, 43 (3), pp.35202. 10.1088/0953-4075/43/3/035202 . hal-00569865

**HAL Id: hal-00569865**

**<https://hal.science/hal-00569865>**

Submitted on 25 Feb 2011

**HAL** is a multi-disciplinary open access archive for the deposit and dissemination of scientific research documents, whether they are published or not. The documents may come from teaching and research institutions in France or abroad, or from public or private research centers.

L'archive ouverte pluridisciplinaire **HAL**, est destinée au dépôt et à la diffusion de documents scientifiques de niveau recherche, publiés ou non, émanant des établissements d'enseignement et de recherche français ou étrangers, des laboratoires publics ou privés.

# Signatures of projectile–nucleus scattering in three-dimensional (e, 2e) cross sections for argon

Xueguang Ren,<sup>1</sup> Arne Senftleben,<sup>1</sup> Thomas Pflüger,<sup>1</sup> Alexander Dorn,<sup>1</sup> Klaus  
Bartschat,<sup>2</sup> Joachim Ullrich<sup>1</sup>

<sup>1</sup>*Max-Planck-Institut für Kernphysik, Saupfercheckweg 1, 69117 Heidelberg,  
Germany*

<sup>2</sup>*Department of Physics and Astronomy, Drake University, Des Moines, Iowa 50311,  
USA*

## Abstract

Electron impact ionization ( $E_0 = 195$  eV) of the 3p-orbital in Argon is investigated experimentally and theoretically. The triple-differential cross sections (TDCS) obtained using a multi-particle momentum spectrometer (reaction microscope) cover more than 80 % of the full solid angle for the slow emitted electron up to an energy of 25 eV and a range of projectile scattering angles from  $-5^\circ$  to  $-15^\circ$ . Inside the projectile scattering plane the TDCS shape is in rather good agreement with a hybrid distorted-wave plus  $R$ -matrix (DWBA-RM) calculation. Outside the scattering plane relatively strong electron emission is observed which is reproduced by theory in magnitude but not in shape. A systematic study of the TDCS behavior and structure in this region indicates that its origin lies in high-order projectile–target interaction.

## 1. Introduction

Atomic and molecular ionization by charged particle impact is one of the most fundamental many-body reactions in physics. Kinematically complete studies on electron impact, also called (e,2e) experiments were feasible already 40 years ago [1, 2] giving very detailed insight into the collision dynamics and target structure studies. On the one hand, the structure of many-body systems can be studied by probing the target's electron momentum density directly via electron impact (e, 2e) and photon

impact ( $\gamma, e\gamma$ ) experiments, see e.g. [3-7] and references therein for more details. On the other hand, a large number of experiments for various target atoms have been performed over the years to gain insight on collision dynamics, see e.g. [8, 9]. These studies were mostly restricted to the so-called coplanar geometry where the incoming projectile and both outgoing electrons move in a common plane and emission angles of the ejected electron in the vicinity of the binary and recoil peaks, since these features were assumed for a long time to contain all the relevant physics of the reaction. The agreement between state-of-the-art theories and experimental data for this kinematics has been steadily improving, especially for simple atomic targets such as hydrogen and helium [10-12]. Recent experimental advances enable the observation of the full coplanar angular range using magnetic angle changers, see e.g. [13, 14] or even the coverage of the full solid angle using reaction microscopes [15, 16]. The latter technique enabled kinematically complete studies of ion impact [17], where for the first time strong electron emission outside the projectile scattering plane was discovered as consequence of the immense phase space acceptance [18]. Up to the present day, theory cannot reproduce these results consistently. A likely mechanism vividly discussed in the literature is high-order projectile–target scattering, which becomes particularly important for small impact parameter collisions [19]. Recently, the measurements of doubly differential cross sections (DDCS) for three-body collision dynamics of proton impact ionization of atomic hydrogen were obtained and reveal again the importance of accurate description of projectile–target interaction [20]. This interpretation was also supported by studies on electron impact ionization where similar out-of-plane structures were observed for helium [16, 21]. Here, theories treating projectile–target interaction beyond first order and non-perturbative calculations [12] were able to reproduce the experimental data at least for large momentum transfer.

Interestingly, discrepancies between all calculations and experiment remain for small momentum transfer. Since high-order projectile–target scattering contributions should be more important for high atomic numbers, studies on heavy targets are timely. However, there is only one recent study focussing on this issue for magnesium,

where the cross-section values on a cone around the momentum-transfer direction were recorded [22]. Calculations are able to reproduce the experimental data qualitatively if the projectile–ion interaction at close distances is taken into account within a distorted-wave model [23, 24]. In other (e, 2e) experiments on argon, for example in the ionization of the 2p orbital ( $E_0 = 5.7$  keV) experimental results emphasize the importance of high-order electron–electron interaction [25].

The present study deals with single ionization of  $\text{Ar}(3p^6\ ^1S)$  covering a large part of the full solid angle for the emitted electron. Most of the previous experiments for electron impact single ionization of argon in the 3p-shell were performed within the scattering plane at various collision kinematics, see e.g. [26-31] and review articles [8, 9]. Experiments examining out-of-plane geometries are scarce. Murray *et al.* [32] performed measurements for symmetric scattering geometries, where the incoming projectile beam was moved out of the plane defined by the two outgoing electrons which had symmetric emission angles and the same energy. Hong *et al.* [33] examined the symmetry of the binary and recoil lobes in-plane and also out-of-plane for 100 eV impact energy.

Here we present 3D-images for electron emission after single ionization of argon at 195 eV impact energy and compare these with respective calculations. A set of cross sections was obtained with the projectile scattering angle varying from  $-5^\circ$  to  $-15^\circ$ , and the ejected electron energy changing from 5 to 25 eV. Our study demonstrates strong electron emission perpendicular to the projectile scattering plane. Furthermore, signatures in the cross section pattern are found that directly point to high-order projectile–ion interaction. Our experiments are compared to calculations within a hybrid first- and second-order Born plus  $R$ -matrix (close-coupling) approach. Past experimental studies within the scattering plane demonstrated that this model considers the essential physics of electron–argon scattering and is in rather good agreement with the experimental data [29].

## 2. Experiment

The experiment was performed using a highly efficient reaction microscope which

was especially designed for electron impact experiments. One of its central features is the direct detection of the fast scattered electron  $e_1$  in coincidence with the slow ejected electron  $e_2$  and the recoiling ion. Therefore, the scattering plane and the momentum transfer are determined directly without relying on their reconstruction by means of the recoil ion momentum as it has to be done using standard reaction microscopes used for ion impact ionization studies. Since for a given target gas temperature the particles' momentum spread increases with the square root of the atomic mass, the recoil ion momentum resolution deteriorates by a factor of more than three in going from the light helium to the heavy argon target. Therefore, the Cold Target Recoil Ion Momentum Spectroscopy (COLTRIMS) technique does not provide sufficient resolution for heavy target species such as argon.

Details of the experimental setup and procedure were described elsewhere [34, 35]. Briefly, a well-focused (1 mm), pulsed electron beam (pulse length  $\approx 1.5$  ns, repetition rate 180 kHz,  $\approx 10^4$  electrons/pulse), produced by a standard thermocathode gun, crosses an argon gas jet (1 mm diameter,  $10^{12}$  atoms/cm<sup>3</sup>), which is produced in a two-stage supersonic gas expansion. Using uniform electric and magnetic fields, the fragments in the final state are projected onto two position- and time-sensitive multi-hit detectors equipped with fast delay-line readout. From the positions of the hits and the times of flight (TOF), the vector momenta of the detected particles can be calculated. It should be noted that the projectile beam axis (defining the longitudinal direction) is adjusted exactly parallel to the electric and magnetic extraction fields. Therefore after passing the target gas jet it arrives at the centre of the electron detector where a central bore in the multi-channel plates of the forward electron detector allows the non-deflected electrons to pass without inducing a hit. In this way, a large part of the full solid angle is covered, 100% for the recoil ion and 80% for secondary electrons below  $E_2 = 25$  eV. As mentioned above, the collision kinematics is directly determined from the two detected electrons not relying on the recoil ion momentum. The electron momentum resolution depends on how well the time and position of the ionizing collision can be determined and, therefore, mainly from the temporal pulse width and the focus diameter of the projectile beam in the target. For the present focus

diameter of 1 mm and the pulse width of 1.5 ns the momentum resolution of electrons is better than 0.1 a.u. As result for the angular resolution the following upper limits are obtained (full-width-at-half-maximum, FWHM):  $\Delta\phi = 6^\circ$  for the azimuth angles of both the fast and slow final state electrons and  $\Delta\theta_1 = 2^\circ$  and  $\Delta\theta_2 = 6^\circ$  for the polar angles of the fast and slow electrons, respectively.

The present kinematical conditions with an impact energy of  $E_0 = 195$  eV are very close to those of Stevenson *et al.* [29] with  $E_0 = 200$  eV, where the coplanar experiments are performed for the scattering angle of  $-15^\circ$ . Hence consistency checks of the cross sections obtained can be performed at least for the coplanar geometry recorded in their experiment. An example is shown in figure 1c) for 10 eV ejected electron energy and  $-15^\circ$  projectile scattering angle. Since both measurements are relative, they are normalized to each other in the binary peak region. The agreement in the cross section shape is quite satisfactory. There is a slight discrepancy only around  $240^\circ$  where the present results are slightly higher than the data from Stevenson *et al.*

### 3. Theory

The theoretical and computational method for the hybrid distorted-wave plus  $R$ -matrix (DWBA-RM) approach was outlined in several papers before [36-40] and hence will not be repeated here. The basic idea is to describe a “fast” projectile by a distorted wave, but the initial bound state and the (slow) ejected-electron–residual-ion interaction *via* an  $R$ -matrix (close-coupling) expansion [36]. Exchange effects between the projectile and the target are neglected in the model, and their inclusion would be non-trivial due to the fundamentally different treatment of the two electrons involved in the process. However, second-order effects in the projectile–target interaction can be accounted for, albeit after some simplifying assumptions [37].

The principal advantage of the hybrid DWBA- $R$ -matrix approach is the fact that it is a *general* method accompanied by a *general* (non-relativistic) computer code [38]. Hence, it does not rely on either exact (as in atomic hydrogen) or often very specialized (as in helium) descriptions of the initial target bound state or the final

ionic states. Instead, multi-configuration expansions may be employed to describe these states. Furthermore, exchange between the (slow) ejected electron and the target is treated *exactly* (in a numerical sense), i.e., it is neither neglected nor simplified via a local potential approximation. Finally, channel-coupling effects (again for the slower of the two outgoing electrons, where they are most important) are accounted for as well.

The specific DWBA-RM calculations for the present work were performed in the model described by Bartschat and Vorov [39]. For the initial bound state and the ejected-electron–residual-ion interaction and the initial bound state, we started with the two-state approximation proposed by Burke and Taylor [40] for the corresponding photoionization problem. Due to the different selection rules for charged-particle impact ionization, however, we allowed for total orbital angular momenta  $L = 0–6$  in the  $e\text{-Ar}^+$  scattering state. Multi-configuration expansions were employed for the initial  $(3s^23p^6)^1S$  bound state as well as for the  $(3s^23p^5)^2P$  and  $(3s3p^6)^2S$  states of  $\text{Ar}^+$ . The latter two states were closely coupled to describe the  $e\text{-Ar}^+$  half-collision problem between the ejected electron and the residual ion. Finally, the projectile–target interaction was described by calculating distorted waves for the projectile in the static potential of the initial target state and then using them to calculate first- or second-order matrix elements as described in [37].

#### 4. Results

Figure 1a) and b) exhibit the experimental and theoretical fully differential cross sections as three-dimensional polar plots for  $\theta_1 = -15^\circ$  scattering angle of the fast final state electron as function of the emission direction of a slow ejected electron with  $E_2 = 10$  eV energy. The projectile is coming in from the bottom ( $\mathbf{k}_0$ ) and scattered to the left ( $\mathbf{k}_1$ ). These two vectors define the scattering plane indicated by the dashed frame in a). In these 3D-plots, the relative FDCS for a particular direction is given as the distance from the origin of the plot to the point on the surface, which is intersected by the ionized electron’s emission direction. The kinematics chosen displays exemplarily the principal features of the emission pattern: It is governed by the

well-known binary and recoil lobes. The binary lobe is oriented along the momentum transfer  $q$  corresponding to electrons emitted in a single binary collision with the projectile. In the opposite direction the recoil lobe is found, where the outgoing slow electron additionally backscatters in the ionic potential. The binary peak shows a minimum along the momentum transfer direction. This is characteristic for ionization of a  $p$ -orbital close to Bethe ridge conditions where the transferred momentum  $q$  is close to the ejected electron's momentum. If the ion remains a pure spectator in the collision then the electron can only be ejected in such a manner if it is initially at rest. This is never the case for a  $p$ -orbital having a node at the origin in momentum space. Since in the present medium to low energy regime the ion always participates in the collision dynamics the minimum is partly filled even for perfect Bethe kinematics. Another striking feature is the relatively large cross section in the angular range in between the binary and recoil lobes.

Regarding the general shape, the agreement with the DWB2-RM theory which includes second-order projectile–target interaction is quite satisfactory. It is known from previous studies [29] that, in order to reach this accuracy, a proper treatment of the target properties resulting from its many-electron character, such as exchange and channel-coupling, is mandatory. In figure 1c) and d) cuts through the 3D-patterns are shown for the projectile scattering plane and the perpendicular plane indicated by the dashed and dotted frames in figure 1a), respectively. Since the experimental results are relative the data shown here and in all following figures have been normalized to the DWB2-RM values at the binary peak (second peak when there is a double peak) using the coplanar cut. Good agreement between theory and experiment concerning the shape of the cross section in the scattering plane is obvious. While the second-order calculation yields a slightly better binary-recoil peak ratio compared to the first-order theory, there is an overestimation of the cross section in the vicinity of the scattered projectile direction around  $300^\circ$ - $360^\circ$ . Both can be attributed to post-collision interaction (PCI) between the two outgoing electrons that – although partially accounted for in the second-order treatment – is still not included in the theory to sufficient accuracy. Stronger discrepancies are seen in the perpendicular

plane (figure 1d) between the binary and recoil lobes, where the experimental data are consistent with a double-peak structure above (0-180° region) and below the scattering plane (180°-360°). Theory, on the other hand, shows just one maximum on each side peaking close to the forward direction. Hints on the underlying mechanisms and the origin of the discrepancies are obtained from the following systematic examination of the cross section behaviour for different projectile scattering angles and ejected electron energies.

In figure 2, 3D-cross sections are plotted for an ejected electron energy of  $E_2 = 15$  eV ( $k_2 = 1.05$  a.u.) and three different scattering angles of  $\theta_l = -5^\circ$ ,  $-10^\circ$  and  $-15^\circ$ , corresponding to the momentum transfers  $q = 0.44$ ,  $0.70$  and  $1.00$  a.u., respectively. The experimental (left column) and DWB2-RM theoretical (right column) 3D-plots again show the dominant binary and recoil lobes with a minimum along  $q$  starting to appear only for the case of large scattering angles. While the general agreement between theory and experiment is good, differences are the slightly flattened shape of the experimental binary lobe and a significantly higher cross section between the binary and recoil lobes, in particular at  $\theta_l = -5^\circ$  and  $-10^\circ$  (a, b). The cross-section cuts in figure 3 show a fairly good agreement, especially with the second-Born theory, inside the scattering plane (left column). The flattened binary lobe in the 3D-representation here corresponds to a more narrow profile with the rising slope shifted to larger angles compared to theory. This is again consistent with PCI and is modelled better by the second-order calculation. Interestingly, this calculation is quite satisfying concerning the observed peak heights at large momentum transfers in the perpendicular plane (figure 3f). However, the remaining difference in the angular position could be caused by the repulsion between the two outgoing electrons, which should give rise to a certain suppression of the cross section along the forward direction and a shift of the structures to larger angles in the perpendicular plane as well. On the other hand, the deviations of the theoretical results from the experimental data increase with decreasing momentum transfer, while the considerable underestimation of the cross section in the  $90^\circ/270^\circ$  region in between the binary/recoil peaks questions a sole PCI effect. Nevertheless, the second-order

calculation is always in better agreement with experiment compared to the first-order model thus pointing again to the importance of high-order effects due to projectile-ion or projectile–ejected-electron interaction. Thus, the question remains which role the projectile–ion interaction plays concerning the perpendicular plane cross section.

Important information is obtained from figure 4 where for a fixed scattering angle of  $\theta_1 = -10^\circ$  cross sections for a range of ejected electron energies  $E_2 = 5, 10, 15, 20$  and  $25$  eV are shown. One can see from the scattering plane data (figure 4, left column) going from large to small energy  $E_2$  that the binary peak changes from a single to a double peak structure. As discussed above, this is due to the Bethe ridge condition being closely fulfilled for  $E_2 = 10$  eV ( $p_2 = 0.86$  a.u.) and even more for  $E_2 = 5$  eV ( $p_2 = 0.61$  a.u.) with  $q = 0.69$  a.u. and  $0.67$  a.u., respectively.

Again, the DWB2-RM calculation agrees well with the experimental cross sections in the binary lobe, except for a certain shift to larger angles that is particularly pronounced for high energies (15 eV, 20 eV and 25 eV). The recoil lobe on the other hand is too low in all cases. Very intriguing is the behaviour of the experimental cross section in the perpendicular plane (figure 4, right column) where a single peak above and below the scattering plane is present for energies  $E_2 = 15$  eV and higher. Theory, being in not too bad agreement at  $E_2 = 25$  eV, again underestimates the cross section at lower energies. For  $E_2 \leq 10$  eV, the perpendicular-plane maxima start to split and develop a pronounced double-peak structure at 5 eV similar to the binary peak. According to our measurements, the perpendicular-plane structure is closely related to the binary-peak structure. This is also confirmed by figure 1 where both, in the experimental 3D-image (a) and the perpendicular-plane cut (d) a double-peak structure is seen consistent with the structure of the binary peak. The angular position of the out-of-plane minimum with respect to the forward direction is exactly the same as for the binary peak minimum. These observations certainly suggest that inelastic collisions where the projectile subsequently scatters elastically with the ion core contribute to a considerable fraction of the cross section perpendicular to the scattering plane. As was already speculated by Schulz *et al.* [18], these would turn the observed scattering plane with respect to the scattering plane of the knock-out collision and thus redistribute part of the binary intensity to other directions around the projectile beam axis. Theory, on the other hand, is not showing any indication of

this pattern. In principle, this mechanism is included in the second-order model, since an integration over all possible scattering directions in the intermediate state is performed. Hence, we do not have an explanation for these deviations at the current time, other than the approximations made in the model that are not directly related to this mechanism.

## 5. Conclusions

We have studied electron impact ionization of Ar( $3p^6\ ^1S$ ) presenting experimental and theoretical 3D-emission patterns for the slow final-state electron. In addition to the binary and recoil lobes, which previously were intensely studied for the projectile scattering plane, we observe a filling of the cross section minimum in between both lobes that is particularly strong for electron emission perpendicular to the projectile scattering plane. Two new observations support the interpretation of this being the result of high-order projectile–target interactions, i.e., an elastic scattering process in the target potential in addition to the electron knock-out collision. Firstly, the relative magnitude of the out-of-plane cross section compared to the first-order binary and recoil peaks is larger when compared to the previously studied helium target [16, 21]. Therefore, there is increased projectile–ion scattering strength due to the higher nuclear charge and larger electron cloud of argon.

Secondly, the structure of the binary lobe consisting of a single peak off the Bethe-ridge kinematics and of two peaks with a minimum in between close to Bethe ridge conditions is directly replicated to the structure of the perpendicular-plane cross section. A possible source is collisions with additional projectile–ion scattering which can redistribute intensity from the scattering plane into other directions.

Given the complexity of the target and the fairly low collision energy of 195 eV, the overall agreement of the DWB2-RM theory is reasonable. At large scattering angles as well as for high energies of the emitted electron, even the perpendicular-plane cross section is reproduced — except for a slight shift that can be explained by PCI not being treated accurately enough in the model. Therefore, the essential physics including the high-order projectile–ion scattering is, in principle,

taken into account in the theory. On the other hand, for small scattering angles and low ejected-electron energies larger discrepancies appear. In particular the double-peak structure in the perpendicular-plane geometry is not reproduced by the calculation.

### **Acknowledgments**

The work of KB was supported by the United States National Science Foundation under grant PHY-757755.

XR is grateful for support from DFG project No. RE 2966/1-1.

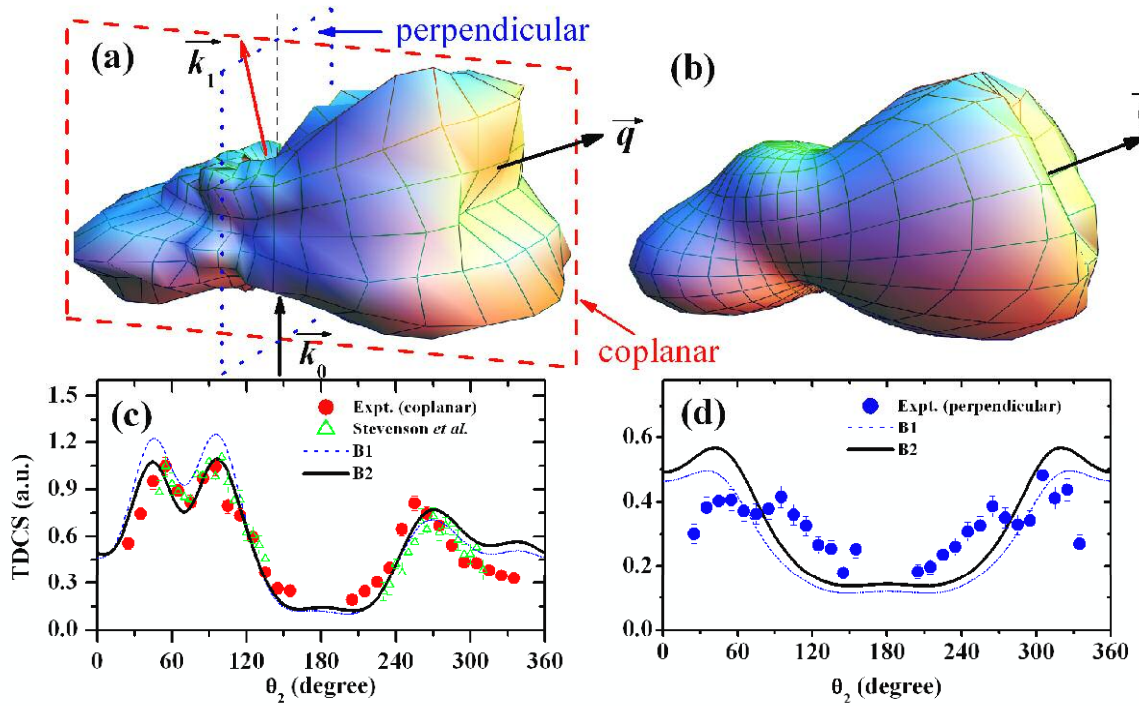
## References

- [1] Ehrhardt H, Schulz M, Tekaas T and Willmann K 1969 *Phys. Rev. Lett.* **22** 89
- [2] Amaldi U, Egidi A, Marconero R and Pizzella G 1969 *Rev. Sci. Instrum.* **40** 1001
- [3] Kaplan I G., Barbiellini B and Bansil A 2003 *Phys. Rev. B* **68** 235104
- [4] Sattler T, Tschentscher Th, Schneider J R, Vos M, Kheifets A S, Lun D R, Weigold E, Dollinger G, Bross H and Bell F 2001 *Phys. Rev. B* **63** 155204
- [5] Brion C E 1986 *Int. J. Quantum Chem.* **29** 1397
- [6] Coplan M A, Moore J H and Doering J P 1994 *Rev. Mod. Phys.* **66** 985
- [7] E. Weigold and I.E. McCarthy 1999 *Electron Momentum Spectroscopy* (Kluwer/Plenum, New York)
- [8] Ehrhardt H, Jung K, Knoth G and Schlemmer P 1986 *Z. Phys. D* **1** 3
- [9] Lahmam-Bennani A 1991 *J. Phys. B* **24** 2401
- [10] Rescigno T N, Baertschy M, Isaacs W A, and McCurdy C W 1999 *Science* **286** 2474
- [11] Bray I 2002 *Phys. Rev. Lett.* **89** 273201
- [12] Colgan J, Foster M, Pindzola M S, Bray I, Stelbovics A T and Fursa D V 2009 *J. Phys. B* **42** 145002
- [13] Read F H and Channing J M 1996 *Rev. Sci. Instrum.* **67** 2372
- [14] Stevenson M A and Lohmann B 2008 *Phys. Rev. A* **77** 032708
- [15] R. Moshhammer, M. Unverzagt, W. Schmitt, J. Ullrich, H. Schmidt-Böcking 1996 *Nucl. Instr. and Meth. B* **108** 425.
- [16] Dürr M, Dimopoulou C, Najjari B, Dorn A and Ullrich J 2006 *Phys. Rev. Lett.* **96** 243202
- [17] Moshhammer R. et al. 1994 *Phys. Rev. Lett.* **73** 3371
- [18] Schulz M, Moshhammer R, Fischer D, Kollmus H, Madison D H, Jones S and Ullrich J 2003 *Nature (London)* **422** 48
- [19] Madison D H, Fischer D, Foster M, Schulz M, Moshhammer R, Jones S and Ullrich J 2003 *Phys.Rev.Lett.* **91** 253201
- [20] Laforge A C, Egodapitiya K N, Alexander J S, Hasan A, Ciappina M F, Khakoo

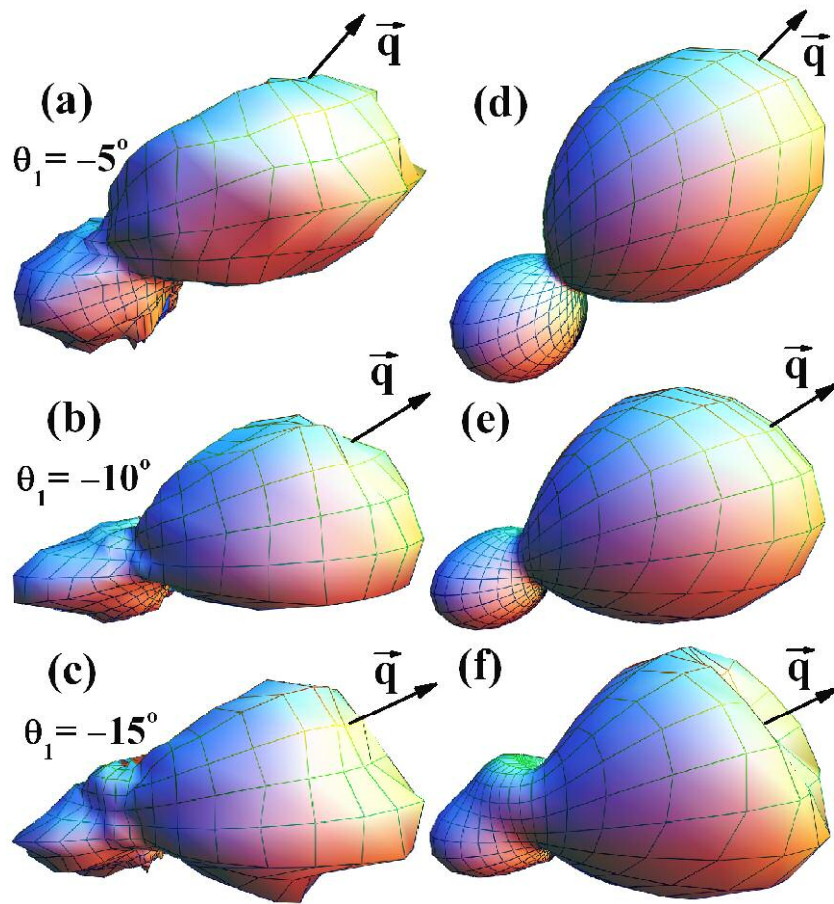
- M A and Schulz M 2009 *Phys. Rev. Lett.* **103** 053201
- [21] Dürr M, Dimopoulou C, Najjari B, Dorn A, Bartschat K, Bray I, Fursa D V, Chen Z, Madison D H and Ullrich J 2008 *Phys. Rev. A* **77** 032717
- [22] van Boeyen R W, Watanabe N, Cooper J W, Doering J P, Moore J H and Coplan M A 2006 *Phys. Rev. A* **73** 032703
- [23] Foster M, Peacher J L, Schulz M, Madison D H, Chen Z and Walters H R J 2006 *Phys. Rev. Lett.* **97** 093202
- [24] Bartschat K, Weflen D and Guan X 2007 *J. Phys. B* **40** 3231
- [25] Taouil I, Duguet A, Lahmam-Bennani A, Lohmann B, Rasch J, Whelan C T and Walters H R J 1999 *J. Phys. B* **32** L5
- [26] Selles P, Mazeau J and Huetz A 1990 *J. Phys. B* **23** 2613
- [27] Ehrhardt H, Hesselbacher K H, Jung K, Schubert E and Willmann K 1974 *J. Phys. B* **7** 69
- [28] Haynes M A and Lohmann B 2001 *Phys. Rev. A* **64** 044701
- [29] Stevenson M, Leighton G J, Crowe A, Bartschat K, Vorov O K and Madison D H 2005 *J. Phys. B* **38** 433; 2007 *Corrigendum: J. Phys. B* **40** 1639
- [30] Avaldi L, Stefani G, McCarthy I E and Zhang X 1989 *J. Phys. B* **22** 3079
- [31] Catoire F, Staicu-Casagrande E M, Nekkab M, Dal Cappello C, Bartschat K and Lahmam-Bennani A 2006 *J. Phys. B* **39** 2827
- [32] Murray A J, Bowring N J and Read F H 2000 *J. Phys. B* **33** 2859
- [33] Hong S P and Beaty E C 1978 *Phys. Rev. A* **17** 1829
- [34] Ullrich J, Moshhammer R, Dorn A, Dörner R, Schmidt L Ph H and Schmidt-Böcking H 2003 *Rep. Prog. Phys.* **66** 1463
- [35] Dürr M, Dimopoulou C, Dorn A, Najjari B, Bray I, Fursa D V, Chen Z, Madison D H, Bartschat K and Ullrich J 2006 *J. Phys. B* **39** 4097
- [36] Bartschat K and Burke P G 1987 *J. Phys. B* **20** 3191
- [37] Reid R H G, Bartschat K and Raeker A, 1998 *J. Phys. B* **31** 563; 2000 *Corrigendum: J. Phys. B* **33** 5261
- [38] Bartschat K, 1993 *Comp. Phys. Commun.* **75** 219
- [39] Bartschat K and Vorov O, 2005 *Phys. Rev. A* **72** 022728

[40] Burke P G and Taylor K T 1975 *J. Phys. B* **8** 2620

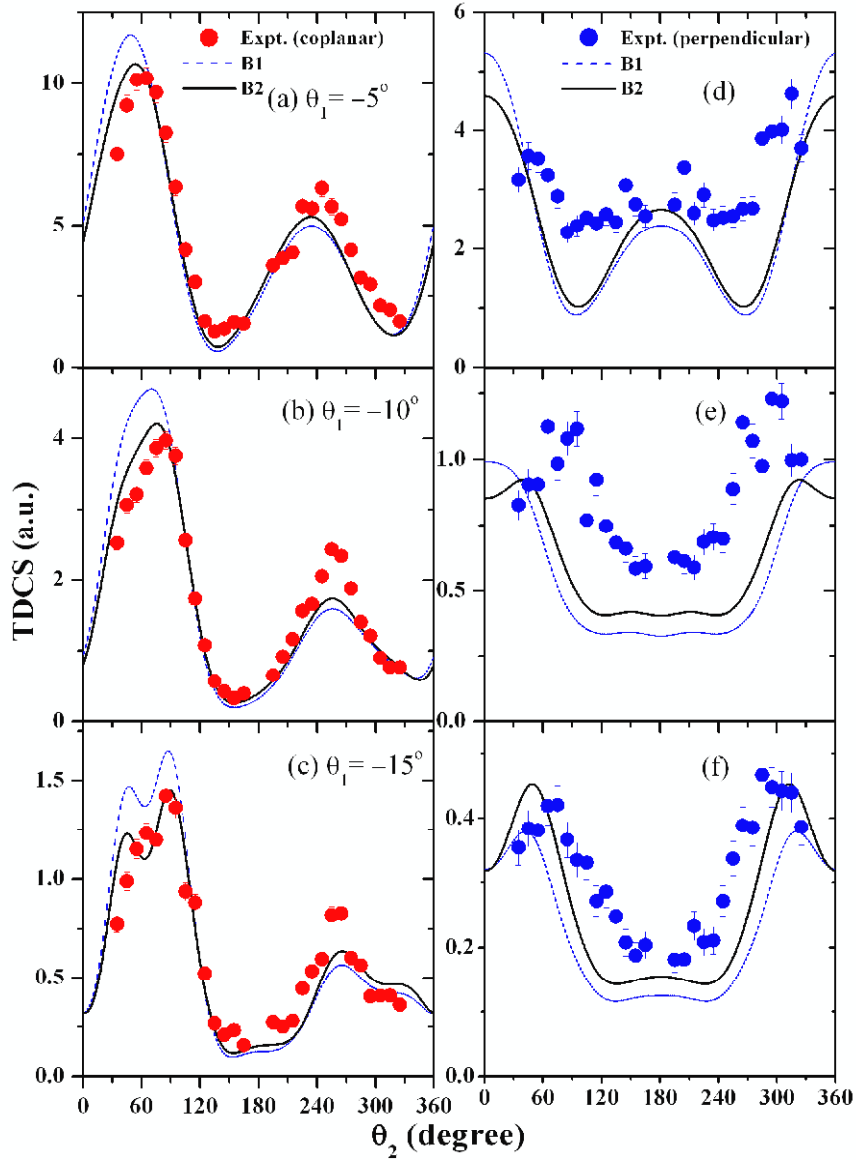
**Figure 1:** Fully-differential cross section (FDCS) as function of the low energetic ( $E_2 = 10$  eV) electron emission angle. The projectile scattering angle is fixed to  $\theta_1 = -15^\circ$  ( $q = 1$  a.u.). a) Experimental 3D-cross section. b) DWB2-RM calculation. c) Cut through the scattering plane indicated by the dashed frame in a). Full circles: present experimental results for  $E_0 = 195$  eV. Open triangles: previous results from Stevenson *et al.* [29] for  $E_0 = 200$  eV. B1 is the first-order DWBA-RM calculation and B2 is the DWB2-RM calculation. d) Cut through the perpendicular plane indicated by the dotted frame in (a). Angular counting starts from the projectile forward direction clockwise.



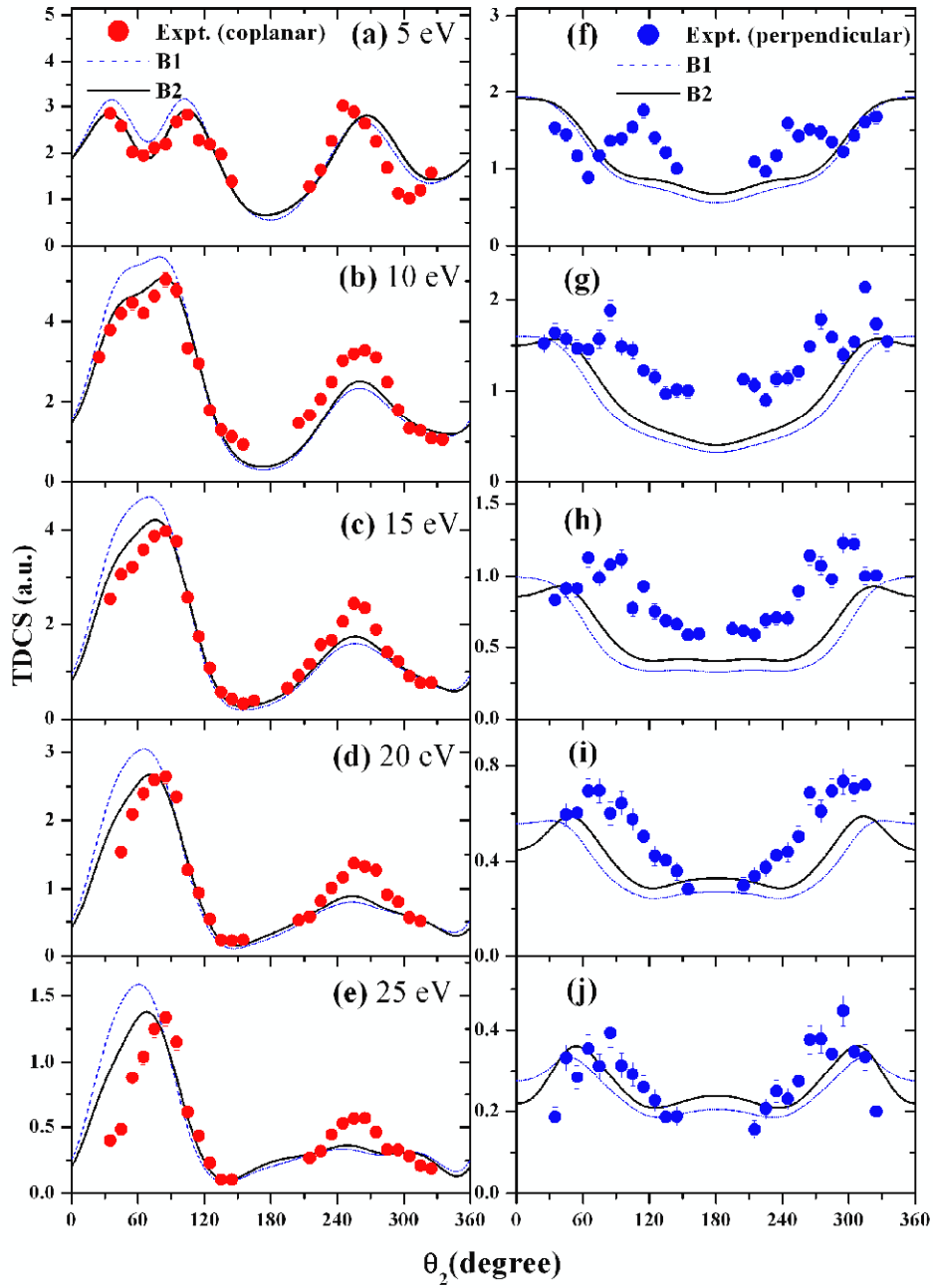
**Figure 2.** Three-dimensional cross sections for  $E_2 = 15$  eV ( $k_2 = 1.05$  a.u.) and different projectile scattering angles  $\theta_1$ . a) and d):  $\theta_1 = -5^\circ$  ( $q = 0.44$  a.u.). b) and e):  $\theta_1 = -10^\circ$  ( $q = 0.7$  a.u.). c) and f)  $\theta_1 = -15^\circ$  ( $q = 1$  a.u.). Left column: experiment. Right column: DWB2-RM theory.



**Figure 3:** Cuts through the 3D-cross sections of figure 2 with  $E_2 = 15$  eV. Left column: FDCS in the projectile scattering plane. Right column: FDCS in the perpendicular plane. a) and d):  $\theta_1 = -5^\circ$ . b) and e):  $\theta_1 = -10^\circ$ . c) and f)  $\theta_1 = -15^\circ$ .



**Figure 4:** FDCS for  $\theta_1 = -10^\circ$  and a range of energies  $E_2$ . Left column: projectile scattering plane. Right column: perpendicular plane. a) and f):  $E_2 = 5$  eV. b) and g):  $E_2 = 10$  eV. c) and h):  $E_2 = 15$  eV. d) and i):  $E_2 = 20$  eV. e) and j):  $E_2 = 25$  eV.



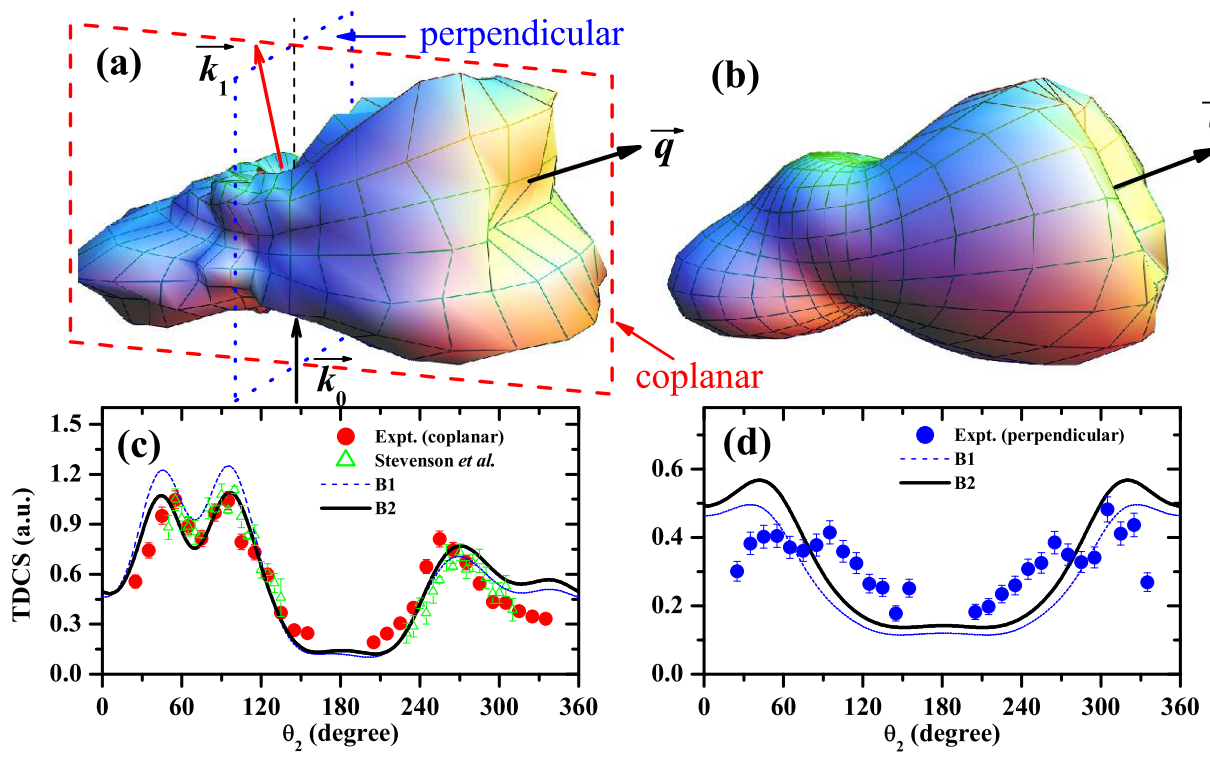


Figure 1 (figure1.eps)

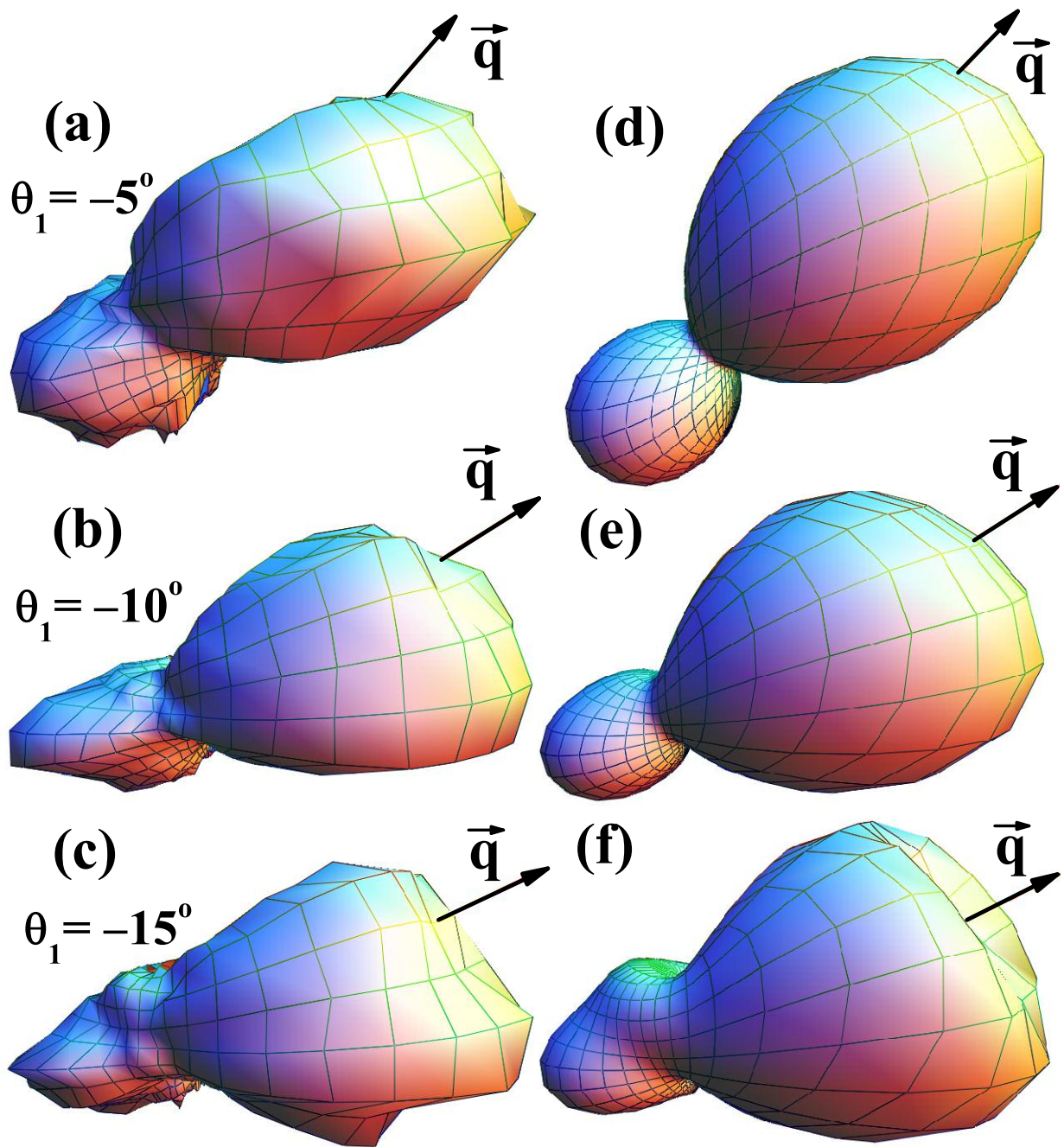


Figure 2 (figure2.eps)

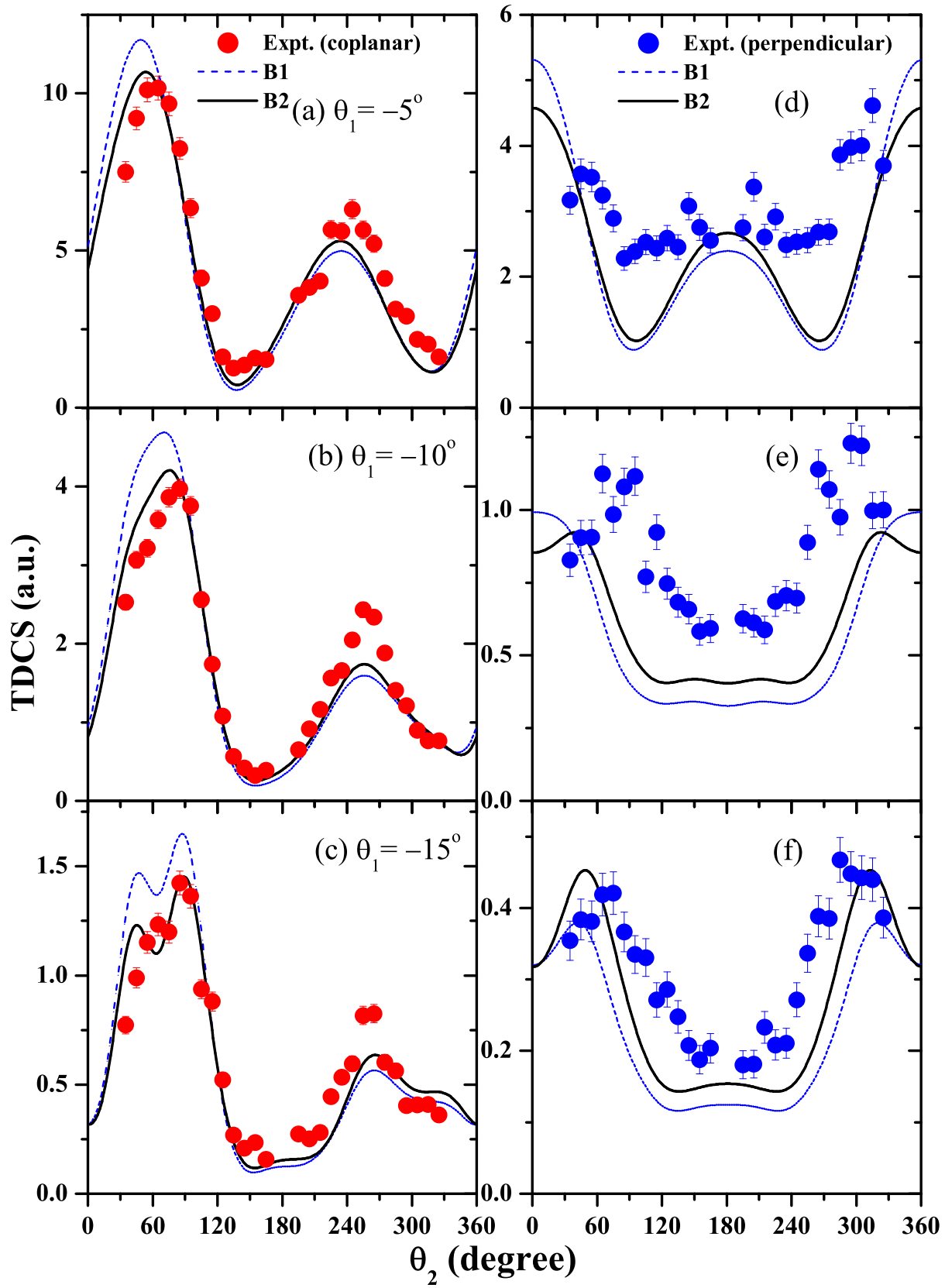


Figure 3 (figure3.eps)

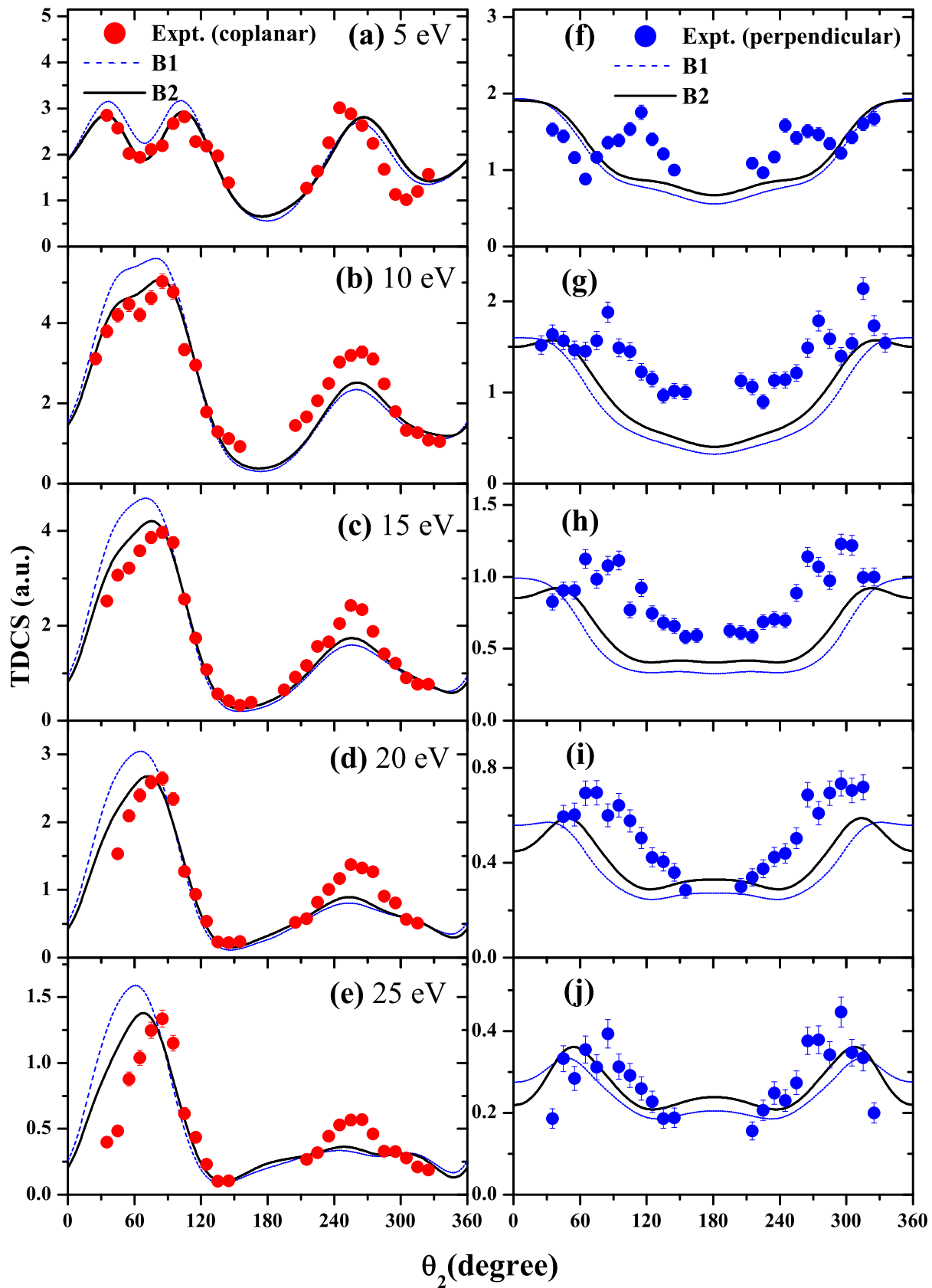


Figure 4 (figure4.eps)